Biointerface Research in Applied Chemistry
Open-Access Journal (ISSN: 2069-5837)

Article
Volume 13, Issue 1, 2023, 72
https://doi.org/10.33263/BRIAC131.072

Preparation and Enhanced Visible-Light Photo-Catalytic Dye Degradation Activity of NiZY Composites

Fethi Ghribi [1,2,3], Amel Boudjemaa [1,*], Zoubir Benmaamar [2,3], Khaldoun Bachari [1]

[1] Centre de Recherche Scientifique et Technique en Analyses Physico-Chimiques, BP 384, Siège ex-Pasna Zone Industrielle, Bou-Ismail CP 42004, Tipaza, Algeria; fethighribi42@gmail.com (F.G.) ; amel_boudjemaa@yahoo.fr (A.B.);bachari2000@yahoo.fr (K.B.);
[2] Laboratoire d'Analyse Fonctionnelle des Procédés Chimiques (LAFPC), Département génie des procédés, Université de Blida 1, Algeria; fethighribi42@gmail.com (F.G.);
[3] Laboratoire des procédés énergétiques et nanotechnologies, Université de Blida 1, Algeria; benmaamarzoubir@yahoo.fr (Z.B.);
* Correspondence: amel_boudjemaa@yahoo.fr (A.B);

Scopus Author ID 24740996500
Received: 12.10.2021; Accepted: 1.11.2021; Published: 2.02.2022

Abstract: The photodegradation of malachite green in water was successfully achieved under LED irradiation in the presence of NiO/zeolite photocatalyst. The photocatalyst was prepared by the impregnation method and characterized by XRD, BET, FTIR, DRs, and SEM techniques. The experiments were investigated by varying factors that influence the malachite green removal, such as adsorption, initial dye concentration, catalyst dose, and pH. The characterization results show that the material exhibited a direct optical transition (1.45 eV). The results indicated that NiO/zeolite shows a synergic effect between adsorption/photocatalysis processes.

Keywords: environment protection; photocatalysis; malachite green;zeolite; NiO; LED light.

1. Introduction

Dyes and pigments are usually used in different industries such as textile, leather tanning, paper, plastics, pharmaceuticals, and foods [1]. Their production and use can be polluted soil and water through the generation of organic dyes, which is a crucial problem to be solved. The discharge of harmful dyes into the water pollutes the water and affects aquatic life [2, 3]. One of the dyes detected in the wastewater is Malachite Green (MG). It is a triphenylmethane dye that is extensively used. It has some damaging effects on the ecosystem, and its contact with skin leads to many problems such as irritation, redness, and pain [4, 5]. Moreover, the dye and organic compounds are also environmentally persistent, and their elimination from wastewater is already reported using various processes such as; photocatalysis [6-8], adsorption [9], ultrasonic irradiation [10, 11], and oxidation [12–14]. On the other hand, MG has a strong absorption band in the visible light region. When released into water bodies, it could reduce transmission of solar light, thereby affecting the aquatic biota of the habitat [15]. Recently, advanced oxidation processes (AOPs) constitute promising, efficient, and environmentally-friendly methods to treat water contaminated by recalcitrant organic pollutants involving the generation of highly reactive radicals [16, 17]. So, photocatalysis in which organic dyes can be degraded into non-toxic inorganic compounds under environmentally friendly conditions is also a green technology [18-20]. The research focus in

this field is mainly on developing an efficient photocatalyst that can work under visible light. Traditional photocatalysts such as TiO_2, ZnO, Ga_2O_3, and $SrTiO_3$ are only able to utilize very limited UV solar photons (ca. 4 %) as a result of their large bandgap energy (Eg > 3 eV). Many attempts have been made to engineer their band structures to match the solar spectrum by coupling two oxides as heterojunction with narrowing Eg or doping metal and non-metal, or constructing heterostructure [21–23]. On such multi-component photocatalysts, the modified materials were often highly dispersed or doped on semiconductor surfaces as nanoparticles, nanoclusters, and mononuclear complexes depending on different preparation methods used [24-26]. NiO photocatalyst is inexpensive compared to other oxides and exhibits chemical stability over a fair pH range [27]. Hence, NiO with a p-type semiconductor is frequently used as a co-catalyst loaded with different photocatalysts. In general, the photocatalysts loaded with NiO exhibited higher efficiencies for photocatalytic water splitting [28]. Also, many reports on NiO nanomaterials with excellent photocatalytic performance are investigated [29-31]. On the other side, it has been proven that supported semiconductors are more effective than unsupported materials [32]. Among supports used are zeolites due to their unique properties [33, 34]. The degradation of organic dyes over TiO_2, NiO, and ZnO-supported zeolite is also studied [35–37]. In addition, many researchers use high-power lamps (100–500 W) as light sources in photocatalytic studies. Very few studies related to low power light irradiation with monochrome are carried out [38]. So, the development of light-emitting diode (LED) in the photocatalysis field has increasingly attracted research attention. The LED light presents several advantages: long lifetime, energy efficiency, high spectral purity, flexible configuration, and small footprint [39]. This work supports NiO onto zeolite Y prepared via an impregnation method and characterized by XRD, BET, FTIR, DRs, and SEM techniques. The prepared material was used for the photodegradation of malachite green. The influences of several parameters were also examined.

2. Materials and Methods

2.1. Preparation of the samples.

The commercial HY zeolite; CBV 760 with SiO_2/Al_2O_3 ratio equal to 60 was purchased from Zeolyst (Table 1). $Ni(NiO_3)_3$, $6H_2O$ was purchased from Fluka, and malachite green powder was purchased from PubChem. NiO/ZY with 5 weight % of NiO was prepared by the impregnation of zeolite with $Ni(NiO_3)_3$, $6H_2O$ precursor. The nickel concentration in the solution was controlled to obtain 5 wt.% of NiO. After stirring at room temperature for 4 h, the product was dried at 80 °C overnight and calcined in air at 400, 500, and 600 °C for 3 h. The samples were labeled Y and 5NiY400, 5NiY500 and 5NiY600, for zeolite alone and modified zeolite calcined at 400, 500, and 600 °C, respectively.

Table 1. Characterization of Zeolite Y.

Zeolystproducts	**SiO_2/Al_2O_3 mole ratio**	**Nominal cation form**	**Na_2O (wt.%)**	**Unit cell size (Å)**	**Surface area (m^2/g)**
CBV 760	60	Hydrogen	0.03	24.24	720

2.2. Characterization techniques.

X-ray diffraction (XRD) was performed with a Bruker D8 diffractometer using Cu Kα radiation in the 2θ interval range of [5 - 80°]. Scanning Electron Microscopy (SEM) images

were performed on FEI Quanta200, and the analyses of the samples were conducted in attached X-rays microanalyses. The chemical composition was obtained using EDS. BET surface area measurements were carried out with micrometric ASAP2010 equipment using nitrogen at 77 K. Before analysis, and the samples were degassed overnight at 200 °C. The Fourier transform infrared (FTIR) spectrum was recorded with a Perkin-Elmer FTIR 1000 spectrometer; the spectrum was recorded in the wavelength range of 400 - 4000 cm^{-1}. The UV-Vis diffuse reflectance (DRS) spectrum was obtained with a Shimadzu UV-2100 spectrophotometer, equipped with an integrating sphere accessory. The obtained reflectance (R %) from the DRS spectrum is used to determine the Eg value. The data were transformed to the extinction coefficient (α) using the equation (1) [40]:

$$\alpha = \frac{(1-R)^2}{2R} \quad (1)$$

2.3. Malachite green removal.

The photocatalytic performance of 5NiY was investigated under visible LED light (12 W) with a major emission at 460 nm was used as a visible light source. The reaction was carried out in the double wallet cylindrical reactor. A catalyst was dispersed in the 200 mL of MG solution. Before irradiation, the mixture was stirred in the dark for 60 min to obtain a good dispersion and establish the adsorption/desorption equilibrium between the catalyst and MG. During the reaction, the mixture's temperature was remained fixed by circulating water using a thermostat bath. Then, the mixture was irradiated by LED lamp placed at 10 cm from the reactor. To examine the concentration change between the initial and the final MG concentration, the absorption spectra were analyzed by a UV-visible spectrophotometer (Carry 50) at 617 nm. The photodegradation efficiencies were calculated according to the following formula:

$$\eta = \frac{C0 - C}{C0} x100 \quad (2)$$

Where η is the photodegradation yield of MG and C_0 and C represent the initial and the final concentration.

3. Results and Discussion

3.1.Material characterization.

The XRD patterns of Y and 5NiY400, 5NiY500, and 5NiY600 materials are regrouped in Figure 1. For different calcination temperatures, Y remained intact after modification (2° < 2θ < 40°), and all the peaks correspond to zeolite Y. This result may be due to the incorporation of Ni particles in the Y pores. Below 2θ = 40°, the peaks intensity decreased and moved to a high angle due to the incorporation of nickel in the Y cage. The typical peaks of NiO are detected at 37.2° and 43.1° (JCPDS No. 71-1179), confirming the doping of NiO on Y [41].

The morphology of all samples is investigated by SEM, and the result is presented in Figure 2. Y has a uniform cubic shape (Figure 2b) and shows agglomerated uniformly shaped particles; the agglomeration maybe due to the interaction of the small particles [42]. EDX results revealed the presence of Si, Al, Na, Ni, and O and the absence of other impurities (Table 2).

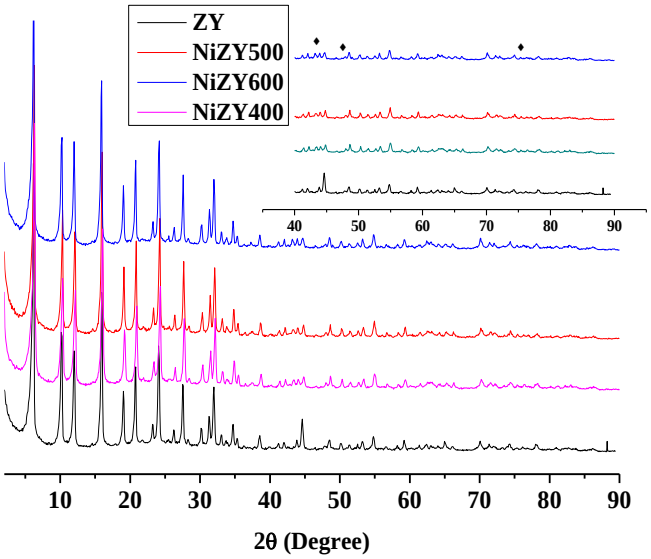

Figure 1. XRD patterns of Y and 5NiY at different calcined temperatures, (♦) NiO.

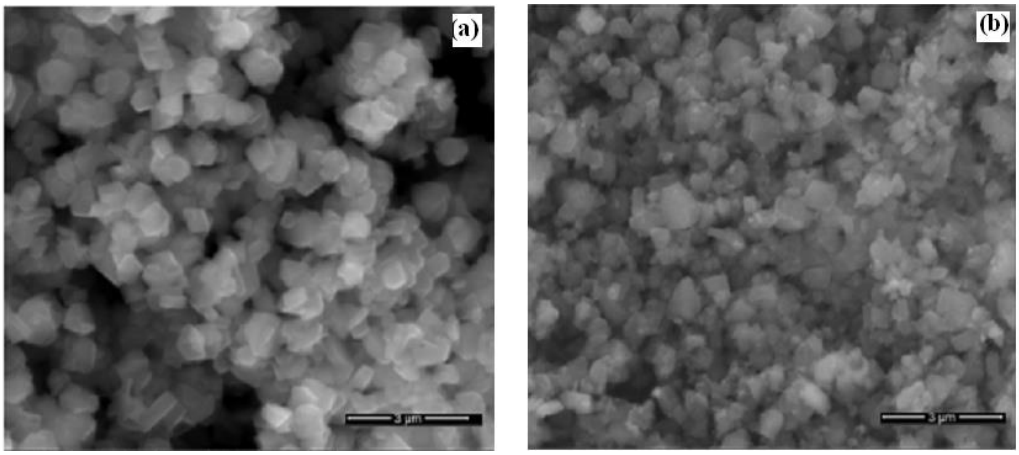

Figure 2. SEM images of **(a)** Y and **(b)** 5NiY.

The surface area, average pore size, and total pore volume are 785.9 m^2/g, 24.7391 Å, and 0.486107 cm^3/g, respectively. The surface area of 5NiY400 is increased because during ion exchange Ni^{2+} replaces two Na^+ [43]. This result may be due to the modification of the textural properties of the material. FTIR spectra of 5NiY at different calcination temperatures are regrouped in Figure 3. The strongest absorption peak at 1050 cm^{-1} was assigned to the framework stretching vibration band of Si(Al)-O of Y [44]. It is observed that the peak is stable during both the ion exchange and also after the calcination process due to the high stability of the zeolite structure and also to the small amount of nickel incorporated into the zeolite structure. However, some small peaks located at 1210 and 828 cm^{-1} are attributed to the Si(Al)-O stretching vibrations [45]. In contrast, the bands located between 460 - 600 cm^{-1} are characteristic of the vibration absorption of Si-O-Si [46]. Pure NiO has absorption peaks at 380 cm^{-1} [47].

Table 2. Elemental composition of ZY sample.

Sample		O	Na	Al	Si	Ni
ZY	**Wt. %**	48.79	11.61	11.03	26.30	-

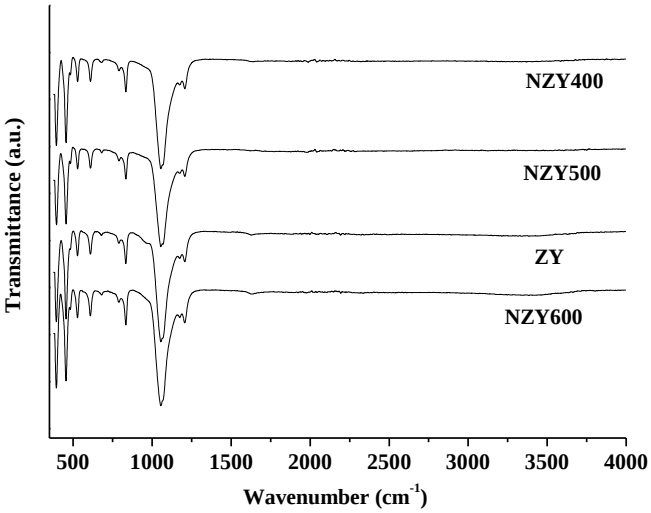

Figure 3. FTIR spectra of 5NiY400, 5NiY500, 5NiY600, and Y samples.

The optical band gap energy of 5NiY600 is determined from the absorption coefficient (α) measured as the incident photon energy function by using the Kubelka-Munk equation (Eq. 1). The Eg value (1.45 eV) is calculated by extrapolation of the linear part of $(\alpha h\nu)^2$ vs. (hν) (Figure 4). Generally, the Eg of nickel oxide is estimated to be 4 eV [48]. Furthermore, reducing the bandgap used NiO as a hetero-system or incorporated into mesoporous materials is important.

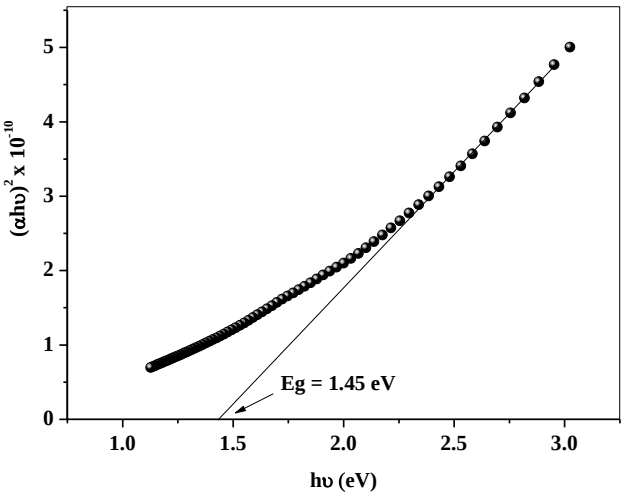

Figure 4. The direct optical transition of 5NiY calcined at 600.

3.2.Photo-degradation of MG dye under LED light.

Photo-catalysis is one of the most important fields for renewable and environment-friendly green energy research. The material used has a semiconductor (SCs) property with narrow bandgap energy located between the valence band (VB) and the conduction band (CB). Generally, the process is based on the light absorption by the SCs, to excite the electrons (e^-) to the CB and leave a hole (h^+) in the VB, thus creating a photo-generated electron/hole (e^-/h^+) pair, responsible for the oxidation and the reduction reactions [49–51]. So, h^+ can react with electron donors in the solution to produce powerful oxidizing free radicals such as hydroxyl radicals, which oxidize the organic molecules. The photo-generation of radical species can be described as follows:

$$NiY + h\nu \rightarrow e^- + h^+ \quad (3)$$

$$e^- + O_2 \rightarrow O_2^{\circ-} \quad (4)$$

$$e^- + O_2^{\circ-} + 2H^+ \rightarrow H_2O_2 \quad (5)$$
$$e^- + H_2O_2 \rightarrow {}^\circ OH + {}^-OH \quad (6)$$
$$H_2O_2 \rightarrow HO_2^- + H^+ \quad (7)$$
$${}^\circ OH + HO_2^- \rightarrow H_2O + O_2^{\circ-} \quad (8)$$
$${}^\circ OH + H_2O_2 \rightarrow H_2O + HO_2^\circ \quad (9)$$

3.3.Synergic between adsorption/photo-catalysis processes.

The photocatalytic activity of 5NiY material is evaluated via the degradation of MG dye under LED light. To do this, 0.25 g/L of the photocatalyst is added to 200 mL of a solution containing 30 mg/L of MG solution at pH 4.6. It is known that the zeolite with a surface area of 785 m^2/g has an adsorption property. For this, the adsorption process of Y and 5NiY is investigated compared to the photocatalysis process. The photolysis test is made in the same conditions before these processes. In the absence of the catalyst, a very lower reactivity is observed. The photolysis of MG is less than 5 %. The adsorption and the photodegradation profiles of both catalysts are shown in Figure 5. This result confirmed the competition between adsorption and photocatalysis processes. Thus, the catalyst is maintained in the dark for 60 min before reaction. As shown results, the photodegradation of MG over 5NiY is higher compared to Y material. MG adsorption over Y is around 48 %, whereas the adsorption increased to 63 % over 5NiY. Furthermore, MG removal is 83 % under LED irradiation. Thus, the enhancement photo-reactivity is due to the interaction between ZY and NiO, leading to an improved contact between catalyst surface and MG dye [52]. Repeated measurement shows almost the same results. Also, ZY used as support prevents the formation of NiO aggregation that increases the surface contact between the photocatalyst and the pollutant and favors an effective photo-excited pairs (e^-/h^+) separation [53, 54].

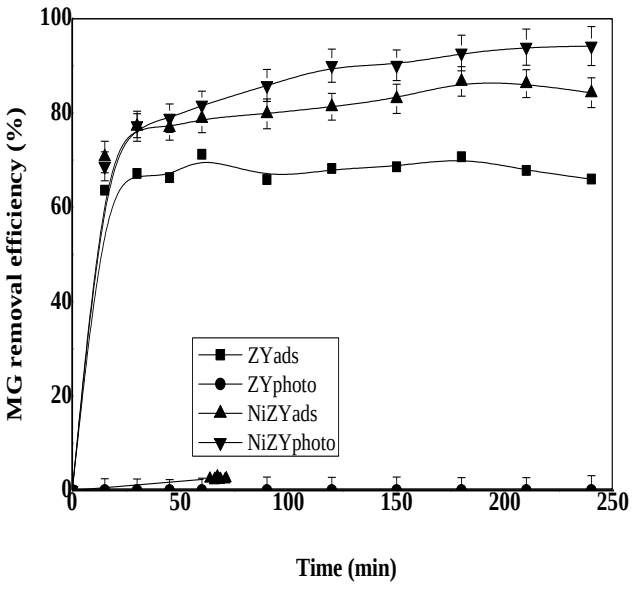

Figure 5. Photo-degradation and adsorption of MG over Y and 5NiY catalysts, under the conditions: [MG] = 20 mg/L, T = 25 °C, pH = 4.6 and catalyst amount = 0.25 g /L under LED lamp (12 Watt).

To determine the optimum MG concentration, various concentrations are used (the varied from 10 to 50 mg/L) (Figure 6). The degradation efficiency after 240 min of irradiation is ~ 92, 94, 63, 74 and 46 % for the concentration 10, 20, 30, 40 and 50 mg/L, respectively. It is also observed for the lower concentration (10 mg/L), the MG removal reached the maximum after the first 15 min of reaction. On the other side, 32 % is obtained with a higher MG

concentration (50 mg/L). It can also be seen. There is a significant decrease in the MG degradation when the MG concentration increases. Also, more MG molecules are available for excitation and energy conversion [55] when the initial concentration increases, requiring more catalyst surfaces for better photodegradation.

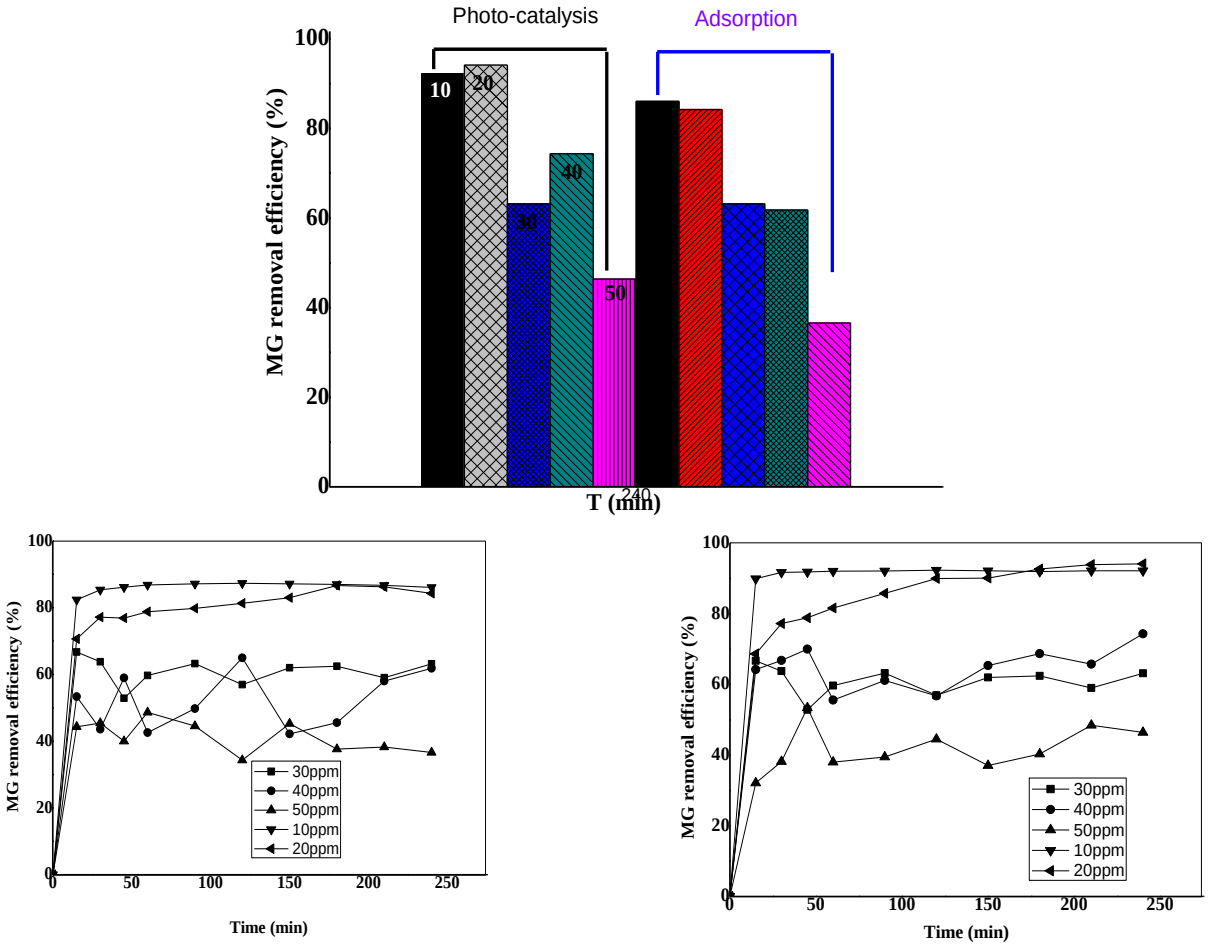

Figure 6. MG concentration effect on the adsorption and photo-degradation processes over 5NiY catalyst, under the conditions: T = 25 °C, pH = 4.6 and catalyst amount = 0.25 g L^{-1} under LED lamp (12 Watt).

The effect of different catalyst amounts on MG degradation is shown in Figure 7. So, the photo-degradation efficiency increased with catalyst concentration and reached to a maximum at 31, 46, 59, 71, 94, 96 and 96 % for 0.12, 0.25, 0.35, 0.5, 0.75, 1 and 1.5 g/L after 240 min of irradiation.

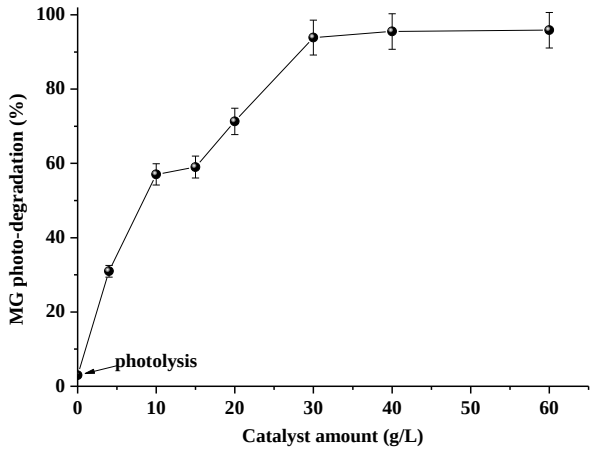

Figure 7. Catalyst dose effect on the photo-degradation of MG (20 mg/L): T = 25 °C, pH = 4.6 under LED light.

Therefore, with the concentrations 0.75, 1, and 1.5 g/L, the MG degradation quickly reached the values 80, 92, and 96 %, respectively, after 60 min of irradiation. Then, at lower catalyst doses (0.12, 0.25, and 0.35 g/L), the degradation as a function of time is unstable, probably due to the presence of a less active site responsible for the light absorption. Heir, the majority of the light has been transmitted into the solution. NiY photocatalyst shows an efficient photoreactivity compared to others materials [56].

To study the effect of pH on the photodegradation of MG, the pH range used is varied from 2 to 9. It is known that the adsorption of dye molecules can influence the pH variation onto the catalyst surface. pH_{PZC} (point of zero charges) is the pH at which the surface of the oxide is uncharged and plays an important role in explaining the adsorption phenomena [57]. In our case, pH_{PZC} is 4.82 measured using the solid addition method. So, the surface charge of the catalyst can be changed depending on the chemical nature of the catalyst and its pH_{PZC}. The results regrouped in Figure 8 show the best photo-reactivity at pH 4.6. At more acidic and basic pHs than pH_{PZC}, the catalyst surface has a positive and a negative charge, respectively [58].

At pH 9 and 8, the repulsive force between the positive charges on the catalyst surface and protonated dye molecules prevents the interaction between them, forming hydroxyl radicals. On the other hand, more hydroxyl anions can be presented in basic pHs leading to the formation of hydroxyl radicals with a good photodegradation of dye through an enhanced (e^-/h^+) separation. But in our case, some contradictory phenomena are observed due to the repulsive forces between the negatively charged catalyst surface and free electrons of MG. In addition, in an acidic medium, low hydroxyl anions are formed a low efficiency. Also, the MG degradation yield decreased in the acidic pH (~ 2) because a higher number of °OH species are recombined to form H_2O_2 and not interacted with MG. It is known that H_2O_2 and HO_2° compounds are appeared due to the reaction of °OH with $^-$OH (reactions 6, 7, and 8). The reactivity of these compounds with organic pollutants is very low compared to °OH. Also, in acidic pH, acidification of the electrolyte by HCl, causes a reaction between Cl^- and °OH conduced to the formation of radical anion $HClO^{\circ -}$ lead to the deactivation of °OH ($Cl^- + {}^\circ OH \rightarrow ClO^{\circ -}H$).

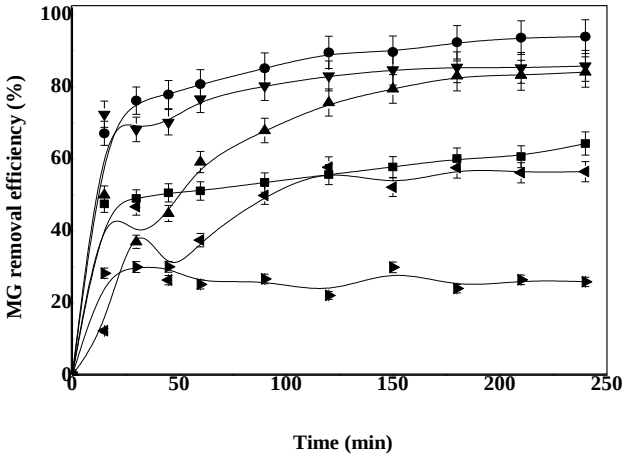

Figure 8. pH effect on the degradation efficiency of MG with: (■) pH 2, (●) pH 4.6, (▲) pH 6, (▼) pH 7, (◄) pH 8 and (►) pH 9 under the conditions: T = 25 °C, catalyst amount = 0.75 g/L and MG concentration = 20 mg/Lunder LED lamp (12 Watt).

4. Conclusions

5NiY has been proved to be an effective photocatalyst for malachite green dye degradation in an aqueous solution. The study was investigated under LED irradiation. The

effects of the initial dye concentration, the catalyst dose, and the pH of the solution were discussed. The detailed characterization technique revealed that the prepared material NiO crystallizes in the zeolite structure. Small bandgap energy makes the material an efficient photocatalyst under visible light irradiation. The combination of zeolite with NiO leads to a high photocatalytic activity for the degradation of malachite green due to the effective separation of (e^-/h^+) generated by the NiY photocatalyst.

Funding

This research received no external funding.

Acknowledgments

This work is supported by the Directorate-General for Scientific Research and Technological Development DGRSDT (Algeria), the authors thanked for their financial support.

Conflicts of Interest

No conflicts of interest.

References

1. Doğan, M.; Abak, H.; Alkan, M. Adsorption of methylene blue onto hazelnut shell: Kinetics, mechanism and activation parameters. *J. Hazard. Mater*. **2009,** *164*, 172–181, https://doi.org/10.1016/j.jhazmat.2008.07.155.
2. Chiong, T.; Lau, S.Y.; Lek, Z.H.;Lek, Z.H.; Koh, B.Y.; Danquah M.K. Enzymatic treatment of methyl orange dye in synthetic wastewater by plant-based peroxidase enzymes. *J. Environ. Chem. Eng*. **2016,** *4*, 2500–2509, https://doi.org/10.1016/j.jece.2016.04.030.
3. Franca, R.D.G.;Vieira, A.; Mata, A.M.T.;Mata, A.M.T.; Carvalho, G.S.; Pinheiro, H.M.; Lourenço, N.D. Effect of an azo dye on the performance of an aerobic granular sludge sequencing batch reactor treating a simulated textile wastewater. *Water Res.* **2015**, *85*, 327–336, https://doi.org/10.1016/j.watres.2015.08.043.
4. Srivastava, S.; Sinha, R.; Roy, D. Toxicological effects of malachite green. *Aquatic Toxic.* **2004**, *66*, 319–329, https://doi.org/10.1016/j.aquatox.2003.09.008.
5. Nethaji, S.; Sivasamy, A.; Thennarasu, G.; Saravanan, S. Adsorption of Malachite Green dye onto activated carbon derived from Borassus aethiopum flower biomass. *J. Hazard. Mater.* **2010**, *181*, 271–280, https://doi.org/10.1016/j.jhazmat.2010.05.008.
6. Santos, R K.; Martins, T.A.; Silva, G. N.; Conceição, M. V. S.; Nogueir,a I. C.;Longo, E.;Botelho, G. Ag3PO4/NiO Composites with Enhanced Photocatalytic Activity under Visible Light. *ACS Omega* **2020**, *5*, 34, 21651–21661, https://doi.org/10.1021/acsomega.0c02456.
7. Guettaıa, D.; Boudjemaa, A.; Zazoua, H.; Mokhtarı, M.; Bacharı, K.. Effıcıent photocatalytıc degradatıon of the pharmaceutical ibuprofen over Fe-FSM-16 photo-catalyst under UV ırradıatıon. Intern.*J. Environ. Studies* **2021**, *78*, 444–458, https://doi.org/10.1080/00207233.2020.1824506.
8. Bousalah, D.; Zazoua, H.; Boudjemaa, A.; Benmounah, A.; Bachari, K.. Degradation of Indigotine food dye by Fenton and photo-Fenton processes. Intern. *J. Environ. Anal. Chem*. **2020**, *14*. https://doi.org/10.1080/003067319.2020.1786546.
9. Beak, M.H.; Ijagbemi, C.O.; Kim, D.S. Treatment of malachite green-containing wastewater using poultry feathers as adsorbent. *J. Environ. Sci. Health, Part A* **2009**, *44*, 536–542, https://doi.org/10.1080/10934520902720132.
10. Behnajady, M.A.; Modirshahla, N.; Shokri, M.; Vahid, B. Effect of operational parameters on degradation of Malachite Green by ultrasonic irradiation. *Ultrasonics Sonochem.* **2008**, *15*, 1009–1014, https://doi.org/10.1016/j.ultsonch.2008.03.004.
11. Benomara, A.; Guenfoud, F.; Mokhtari, M.; Boudjemaa, A. Sonolytic, sonocatalytic and sonophotocatalytic degradation of a methyl violet 2B usingiron-based catalyst. *Reaction Kinet., Mech. Catal.* **2021**, 513–528, https://doi.org/10.1007/s11144-020-01902-9.

12. Liu, Z.; Liu, Z.; Cui, T.;Li, J.; Zhang, J.; Chen, T.; Wang, X.; Liang, X. Photocatalysis of two-dimensional honeycomb-like ZnO nanowalls on zeolite. *Chem. Eng. J.* **2014**, *235*, 257–263, https://doi.org/10.1016/j.cej.2013.09.022.
13. Khataee, A.R.; Vatanpour, V.; Amani Ghadim, A.R. Decolorization of C.I. Acid Blue 9 solution by UV/Nano-TiO2, Fenton, Fenton-like, electro-Fenton and electrocoagulation processes: A comparative study. *J. Hazard. Mater.***2009**, *161*,1225–1233, https://doi.org/10.1016/j.jhazmat.2008.04.075.
14. Zhang, G.; Qin, L.; Meng, Q.;Fan, Z.;Wu, D. Aerobic SMBR/reverse osmosis system enhanced by Fenton oxidation for advanced treatment of old municipal landfill leachate. *Bioresource Techn*. **2013**, *142*, 261–268, https://doi.org/10.1016/j.biortech.2013.05.006.
15. Gokulakrishnan, S.; Parakh, P.; Prakash, H. Degradation of Malachite green by Potassium persulphate, its enhancement by 1,8-dimethyl-1,3,6,8,10,13-hexaazacyclotetradecane nickel(II) perchlorate complex, and removal of antibacterial activity. *J. Hazard. Mater.* **2012**, *213–214*, 19–27, https://doi.org/10.1016/j.jhazmat.2012.01.031.
16. Yang, Y.; Pignatello, J.J.; Ma, J.; Mitch, W.A. Comparison of Halide Impacts on the Efficiency of Contaminant Degradation by Sulfate and Hydroxyl Radical-Based Advanced Oxidation Processes (AOPs). *Environ. Sci.Techn.* **2014**, *48*, 2344–2351, https://doi.org/10.1021/es404118q.
17. Oturan, M.A.; Aaron, J.J. Advanced Oxidation Processes in Water/Wastewater Treatment: Principles and Applications. A Review. *Critical Reviews Environ. Sci. Techn*. **2014,** *44*, 2577–2641, https://doi.org/10.1080/10643389.2013.829765.
18. Khataee, A.; Darvishi Cheshmeh Soltani, R.; Hanifehpour, Y.;Safarpour, M.; Gholipour Ranjbar, H.;Joo, S. W. Synthesis and Characterization of Dysprosium-Doped ZnO Nanoparticles for Photocatalysis of a Textile Dye under Visible Light Irradiation. *Indus.Eng. Chem. Res.* **2014**, *53*,1924–1932, https://doi.org/10.1021/ie402743u.
19. Zhang, M.; Shao, C.; Guo, Z.; Zhang, Z.; Mu, J.; Zhang, P.; Cao, T.; Liu, Y. Hierarchical Nanostructures of Copper(II) Phthalocyanine on Electrospun TiO_2 Nanofibers: Controllable Solvothermal-Fabrication and Enhanced Visible Photocatalytic Properties. ACS Appl. *Mater. Interf.s* **2011**, *3*:369–377, https://doi.org/10.1021/am100989a.
20. Kerchich,S.;Boudjemaa, A.; Chebout, R.; Bachari, K.; Mameri, N. High performance of -Fe2O3 novel photocatalyst supported on LDH structure. *J. Photochem. Photob. A:Chem.* **2021**, *406*, 113001, https://doi.org/10.1016/j.jphotochem.
21. Chen, X.; Shen, S.; Guo, L.; Mao, S.S. Semiconductor-based Photocatalytic Hydrogen Generation. *Chem. Reviewer* **2010,** *110*, 6503–6570, https://doi.org/10.1021/cr1001645.
22. Qi, L.; Yu, J.; Jaronie,c M. Preparation and enhanced visible-light photocatalytic H2-production activity of CdS-sensitized Pt/TiO2 nanosheets with exposed (001) facets. Phys.*Chem. Chem. Phys.* **2011**, *13*, 8915, https://doi.org/10.1039/c1cp20079h.
23. He, X.; Kai,T.; Ding,P. Heterojunction photocatalysts for degradation of the tetracycline antibiotic: a review. Environ.*Chem. Letters* **2021**, https://doi.org/10.1007/s10311-021-01295-8.
24. Gu, Q.; Long, J.; Zhou, Y.;Yuan, R.; Lin, H.; Wang, X. Single-site tin-grafted anatase TiO2 for photocatalytic hydrogen production: Toward understanding the nature of interfacial molecular junctions formed in semiconducting composite photocatalysts. *J. Catal.* **2012**, *289*, 88–99, https://doi.org/10.1016/j.jcat.2012.01.018.
25. Iwaszuk, A.; Nolan, M.; Jin, Q.;Fujishima, M.; Tada, H. Origin of the Visible-Light Response of Nickel(II) Oxide Cluster Surface Modified Titanium(IV) Dioxide. *J. Phys. Chem. C* **2013**, *117*, 2709–2718, https://doi.org/10.1021/jp306793r.
26. Sahoo, S.K.; Bhattacharya, S.; Sahoo, N.K. Photocatalytic degadration of biological recalcitrant pollutants: a green chemistry approach. Biointer. *Res. Appl. Chem*. **2020**, *10*, 5048-5060, https://doi.org/10.33263/BRIAC102.048060.
27. Santos, R. K.; Martins, T. A.; Silva, G. N.; Conceicao, M. V.S.;Nogueira, I. C.; Longo, E.; Botelho, G. Ag3PO4/NiO Composites with Enhanced Photocatalytic Activity under Visible Light. *ACS Omega* **2020**, *5*, 21651−21661, https://doi.org/10.1021/acsomega.0c02456.
28. Ku, Y.; Lin, C.-N.; Hou, W.-M. Characterization of coupled NiO/TiO2 photocatalyst for the photocatalytic reduction of Cr(VI) in aqueous solution. *J. Molec. Catal. A: Chem.* **2011**, *349*,20–27, https://doi.org/10.1016/j.molcata.2011.08.006.

29. Hameeda, B.; Mushtaq, A.; Saeed, M.;Munir, A.; Jabeen, U.; Waseem, A. Development of Cu-doped NiO nanoscale material as efficient photocatalyst for visible light dye degradation. *Toxin Reviews* **2020**, https://doi.org/10.1080/15569543.2020.1725578.
30. Padervand M.; Reza Elahifard M.; Vatan Meidanshahi R.;Ghasemi S.; Haghighi S.; Gholami M. R. Investigation of the antibacterial and photocatalytic properties of the zeolitic nanosized AgBr/TiO2 composites. *Mater. Sci. Semicond. Proc.* **2012**, *15*,73–79, https://doi.org/10.1016/j.mssp.2011.08.008.
31. Akbari, A.; Sabouri, Z.; Hosseini, H. A.; Hashemzadeh, A.; Khatamid, M.; Darroudi, M. Effect of nickel oxide nanoparticles as a photocatalyst in dyes degradation and evaluation of effective parameters in their removal from aqueous environments. *Inorg. Chem. Comm.*. **2020**, *115*, 107867, https://doi.org/10.1016/j.inoche.2020.107867.
32. Woo, S.; Kim, J.; Cho, G.;Kim, K.; Lyu, H.; Kim, Y. Influence of nickel oxide nanolayer and doping in organic light-emitting devices. *J. Indus. Engin. Chem.* **2009**, *15*,716–718, https://doi.org/10.1016/j.jiec.2009.09.051.
33. Amiri, M.; Nezamzadeh-Ejhieh, A. Improvement of the photocatalytic activity of cupric oxide by deposition onto a natural clinoptilolite substrate. *Mater. Sci. Semicond. Proc.* **2015**, *31*, 501–508, https://doi.org/10.1016/j.mssp.2014.12.030.
34. Nezamzadeh-Ejhieh, A.; Khorsandi, M. A comparison between the heterogeneous photodecolorization of an azo dye using Ni/P zeolite and NiS/P zeolite catalysts. *Iranian J. Catal.* **2011**, *1*, 99–104, http://ijc.iaush.ac.ir/article_551253.html.
35. Liu, X.; An, S.; Shi W.;Yang Q.; Zhang L. Microwave-induced catalytic oxidation of malachite green under magnetic Cu-ferrites: New insight into the degradation mechanism and pathway. *J. Molec. Catal. A: Chem.* **2014**, *395*,243–250, https://doi.org/10.1016/j.molcata.2014.08.028.
36. Derikvandi, H.; Nezamzadeh-Ejhieh, A. Comprehensive study on enhanced photocatalytic activity of heterojunction ZnS-NiS/zeolite nanoparticles: Experimental design based on response surface methodology (RSM), impedance spectroscopy and GC-MASS studies. *J. Coll. Inter. Sci.* **2017**, *490*, 652–664, https://doi.org/10.1016/j.jcis.2016.11.105.
37. Petkowicz, D.I.; Pergher, S.B.C.; da Silva, C.D.S.; Novais da Rocha, Z.; João H.Z. dos Santos. Catalytic photodegradation of dyes by in situ zeolite-supported titania. *Chem. Eng. J.* **2010**, *158*, 505–512, https://doi.org/10.1016/j.cej.2010.01.039.
38. Yin, S.; Liu, B.; Zhang, P.;Morikawa, T.; Yamanaka, K.; Sato T. Photocatalytic Oxidation of NO_x under Visible LED Light Irradiation over Nitrogen-Doped Titania Particles with Iron or Platinum Loading. *J. Phys. Chem. C* **2008**, *112*, 12425–12431, https://doi.org/10.1021/jp803371s.
39. Ghosh, J.P.; Langford, C.H.; Achari, G. Characterization of an LED Based Photoreactor to Degrade 4-Chlorophenol in an Aqueous Medium Using Coumarin (C-343) Sensitized TiO_2. *J. Phys.Chem. A* **2008**, *112*, 10310–10314, https://doi.org/10.1021/jp804356w.
40. Tauc, J.; Grigorovici, R.; Vancu, A. Optical properties and electronic structure of amorphous germanium. *Phys.Stat.Solidi (b)* **1966**, *15*,627–637, https://doi.org/10.1002/pssb.19660150224.
41. Choo,M.Y.; Oi, L.E.; Daou, T.J.; Ling, T.C.; Lin, Y.C.; Centi, G.; Ng, E.P.; Juan, J.C. Deposition of NiO nanoparticles on nanosized zeolite NaY for production of biofuel via hydrogen-free deoxygenation. *Materials.* **2020**, *13*, 3104, https://doi.org/10.3390/ma13143104.
42. Husin, H.; Mahidin, M.; Pontas, K.; Ahmadi, A.; Ridho, M.; Erdiwansyah, E.; Nasution, F.; Has fita, F.; Hussin, M. H. Microwave-assisted catalysis of water-glycerol solutions for hydrogen production over NiO/zeolite catalyst. *Heliyon* **2021**, *7*, e07557, https://doi.org/10.1016/j.heliyon.2021.e07557.
43. Nezamzadeh-Ejhieh, A.; Karimi-Shamsabadi, M. Comparison of photocatalytic efficiency of supported CuO onto micro and nano particles of zeolite X in photodecolorization of Methylene blue and Methyl orange aqueous mixture. *Appl. Catal. A: Gen.* **2014**, *477*, 83–92, https://doi.org/10.1016/j.apcata.2014.02.031.
44. Nezamzadeh-Ejhieh, A.; Khodabakhshi-Chermahini, F. Incorporated ZnO onto nano clinoptilolite particles as the active centers in the photodegradation of phenylhydrazine. *J. Indus. Eng. Chem.* **2014**, *20*, 695–704, https://doi.org/10.1016/j.jiec.2013.05.035.
45. Breck, D.W. (1974) Zeolite Molecular Sieves, John Wiley & Sons, New York, https://academic.oup.com/chromsci/article-abstract/13/4/18A/357490.
46. Mohammadyari, P.; Nezamzadeh-Ejhieh, A. Supporting of mixed ZnS–NiS semiconductors onto clinoptilolite nanoparticles to improve its activity in photodegradation of 2-nitrotoluene. *RSC Adv* **2015**, *5*, 75300–75310, https://doi.org/10.1039/C5RA12608H.

47. Sheena, P.A.; Priyanka, K.P.; Sabu, B.; Varghese, T. Effect of calcination temperature on the structural and optical properties of nickel oxide nanoparticles. *Наносистемы: физика, химия, математика* **2014,** *5*, https://cyberleninka.ru/article/n/effect-of-calcination-temperature-on-the-structural-and-optical-properties-of-nickel-oxide-nanoparticles.
48. Wang, Z.; Li, Z.; Sun, J.;Zhang, H.; Wang, W.; Zheng, W.; Wang C. Improved Hydrogen Monitoring Properties Based on p-NiO/n-SnO_2 Heterojunction Composite Nanofibers. *J. Phys. Chem. C* **2010**, *114*, 6100–6105, https://doi.org/10.1021/jp9100202.
49. Shen, H.; Peppel, T.; Strunk J.; Sun, Z. Photocatalytic Reduction of CO2 by Metal-Free-Based Materials: Recent Advances and Future Perspective. *Solar RRL* **2020**, *4*, 1900546, https://doi.org/10.1002/solr.201900546.
50. Radko, M; Kowalczyk, A.; Mikrut, P.; Witkowski, S.; Mozgawa, W.; Macyk, W.; Chmielarz, L. Catalytic and photocatalytic oxidation of diphenyl sulphide to diphenyl sulfoxide over titanium dioxide doped with vanadium, zinc, and tin. *RSC Adv.* **2020**, *10*, 4023-4031, https://doi.org/10.1039/C9RA09903D.
51. Kezzim, A.; Boudjemaa, A.; Belhadi, A.; Trari, M. Photo-catalytic degradation of ibuprofen over the new semiconducting catalyst α-(Cu,Fe)2O3 prepared by hydrothermal route. *Res. Chem. Interm.* **2017**, *43*, 3727–3743, https://doi.org/10.1007/s11164-016-2837-8.
52. Benammar, S.; Boudjemaa, A.; Nezzal, G.; Gómez-Ruiz, S.; Meziane, D.; Bachari, K.; Lounis, A.; Coville, N. J. Nanoparticles based on copper deposited on carbon spheres. Preparation, characterization and application for CO2 photo-electrochemical reduction. *J. Electroan. Chem.* **2018**, *809*, 80–87, https://doi.org/10.1016/j.jelechem.2017.12.007.
53. Karimi-Shamsabadi, M.; Behpour, M.; Babaheidari, A.K.; Saberi Z. Efficiently enhancing photocatalytic activity of NiO-ZnO doped onto nanozeoliteX by synergistic effects of p-n heterojunction, supporting and zeolite nanoparticles in photodegradation of Eriochrome Black T and Methyl Orange. *J. Photochem. Photob. A: Chem.* **2017**, *346*,133–143, https://doi.org/10.1016/j.jphotochem.2017.05.038.
54. Krishnan, T.; Wan Mansor, W. S. Photocatalytic Degradation of Dyes by TiO2 Process in Batch Photoreactor. *Lett. Appl. NanoBiosc.* **2020**, *9*, 1502 – 1512, https://doi.org/10.33263/LIANBS94.15021512.
55. Mora-Seró, I.; Bisquert, J.; Dittrich, Th.;Belaidi, A.; Susha, A.S.; Rogach,A. L.Photosensitization of TiO_2 Layers with CdSe Quantum Dots: Correlation between Light Absorption and Photoinjection. *J. Phys. Chem. C* **2007**, *111*,14889–14892, https://doi.org/10.1021/jp074907w.
56. Topkaya, E.; Konyar, M.; Yatmaz, H.C.; Öztürk, K. Pure ZnO and composite ZnO/TiO2 catalyst plates: A comparative study for the degradation of azo dye, pesticide and antibiotic in aqueous solutions. *J. Coll. Interf. Sci.* **2014**, *430*,6–11, https://doi.org/10.1016/j.jcis.2014.05.022.
57. Nazarkovsky, M.A.; Bogatyrov, V.M.; Czech, B.;Galaburda, M.V.; Wójcik, G.; Kolomys, O.F.; Strelchuk, V.V.;Malysheva, M.L.; Oranska, O.I.Synthesis and properties of zinc oxide photocatalyst by high-temperature processing of resorcinol-formaldehyde/zinc acetate mixture. *J. Photochem. Photob. A: Chem.* **2017**, *334*, 36–46, https://doi.org/10.1016/j.jphotochem.2016.10.040.
58. Babaahamdi-Milani, M.; Nezamzadeh-Ejhieh, A. A comprehensive study on photocatalytic activity of supported Ni/Pb sulfide and oxide systems onto natural zeolite nanoparticles. *J. Hazard. Mater.* **2016**, *318*, 291–301, https://doi.org/10.1016/j.jhazmat.2016.07.012.